

Impedance optimization for EIC

A. Blednykh

September 2019

Collider Accelerator Department
Brookhaven National Laboratory

U.S. Department of Energy

USDOE Office of Science (SC), Nuclear Physics (NP) (SC-26)

Notice: This technical note has been authored by employees of Brookhaven Science Associates, LLC under Contract No. DE-SC0012704 with the U.S. Department of Energy. The publisher by accepting the technical note for publication acknowledges that the United States Government retains a non-exclusive, paid-up, irrevocable, world-wide license to publish or reproduce the published form of this technical note, or allow others to do so, for United States Government purposes.

DISCLAIMER

This report was prepared as an account of work sponsored by an agency of the United States Government. Neither the United States Government nor any agency thereof, nor any of their employees, nor any of their contractors, subcontractors, or their employees, makes any warranty, express or implied, or assumes any legal liability or responsibility for the accuracy, completeness, or any third party's use or the results of such use of any information, apparatus, product, or process disclosed, or represents that its use would not infringe privately owned rights. Reference herein to any specific commercial product, process, or service by trade name, trademark, manufacturer, or otherwise, does not necessarily constitute or imply its endorsement, recommendation, or favoring by the United States Government or any agency thereof or its contractors or subcontractors. The views and opinions of authors expressed herein do not necessarily state or reflect those of the United States Government or any agency thereof.

<p style="text-align: center;">C-AD TECHNICAL NOTE BROOKHAVEN NATIONAL LABORATORY</p>	<p>NUMBER eRHIC/70</p>
<p>AUTHOR: A. Blednykh, M. Blaskiewicz and C. Hetzel</p>	<p>DATE 09/18/2019</p>
<p>TITLE Impedance optimization for EIC</p>	

Abstract
September 18, 2019

This report provides a summary of the longitudinal impedance optimization performed to date for the following vacuum components: pump slots, transition from the octagonal shape of the arc chambers to the circular shape of the straight section chambers and the main detector chamber. The cut off frequency for E_{01} –mode has been estimated for different cross sections of the vacuum chambers. The advantages of using bunch lengthening to decrease the loss factor and reduce the heating effects for the vacuum components is also examined.

1. The cutoff frequency

To eliminate the generation of the Higher Order Modes (HOMs) and minimize their contribution to beam related heating of the vacuum components, the length (σ_s) of the circulating bunch needs to be larger than the radius b of the vacuum chamber, $\sigma_s > b$. For a bunch length $\sigma_s = 12\text{mm}$, the bunch spectrum is generated up to $\sim 8.5\text{GHz}$. In Figure 1, the cutoff frequency as a function of the circular vacuum chamber radius b is shown for the first fundamental longitudinal E_{01} -mode.

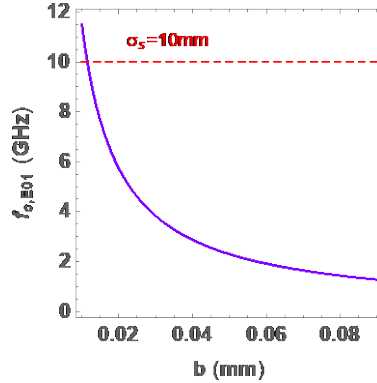


Fig. 1: The cutoff frequency $f_{c,E01}$ for E_{01} -mode vs. the circular vacuum chamber radius b .

For a circular chamber, the cutoff frequency is determined

$$f_{c,E01} = cv_{01}/2\pi b, \quad (1)$$

where c is velocity of light, b is the radius of the circular pipe and $v_{01} = 2.405$ is the root of the Bessel function. The cutoff frequency of a circular vacuum chamber with a $b = 31\text{mm}$ radius (Fig. 2b) is $f_{c,E01} = 3.7\text{GHz}$. The currently proposed arc vacuum chamber has an octagonal shape as shown in Fig. 2a. The cutoff frequency for this geometry has been calculated numerically using the GdfidL code [1], $f_{c,E01}^{oct} = 4.4\text{GHz}$ with a full horizontal aperture of $2a = 82\text{mm}$ and a full vertical aperture of $2d = 40\text{mm}$.

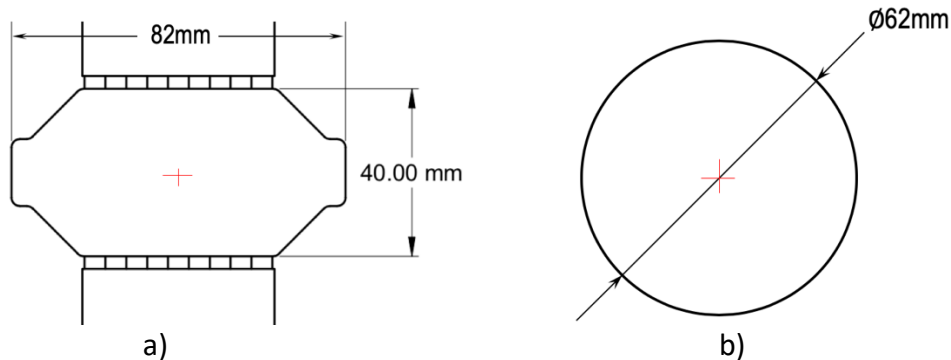


Fig. 2: Current vacuum chamber profiles. a) Arc chamber. b) Straight section chamber.

Based on the analysis of this geometry, the bunch length should be increased by a factor of ~ 3.5 from the present length of 12mm in order to relieve the heat load on the vacuum system resulting from HOMs.

2. Pump Slots

The vacuum chambers in the storage ring will require connections to pumping elements in order to maintain the required operating pressure. These pumps will be separated from the beam channel by slots to minimize detrimental effects to the electron beam. It is important to balance the need for high conductance to the pump with the RF shielding requirements since there will be approximately 500 of these elements in the storage ring. The pump slots will be located on the top and the bottom surface of the beam channel. The first iteration started with a series of 10 slots with a width $w = 5\text{mm}$ and a total length $l = 90\text{mm}$. The distance, between adjacent slots was chosen as $h = 5\text{mm}$.

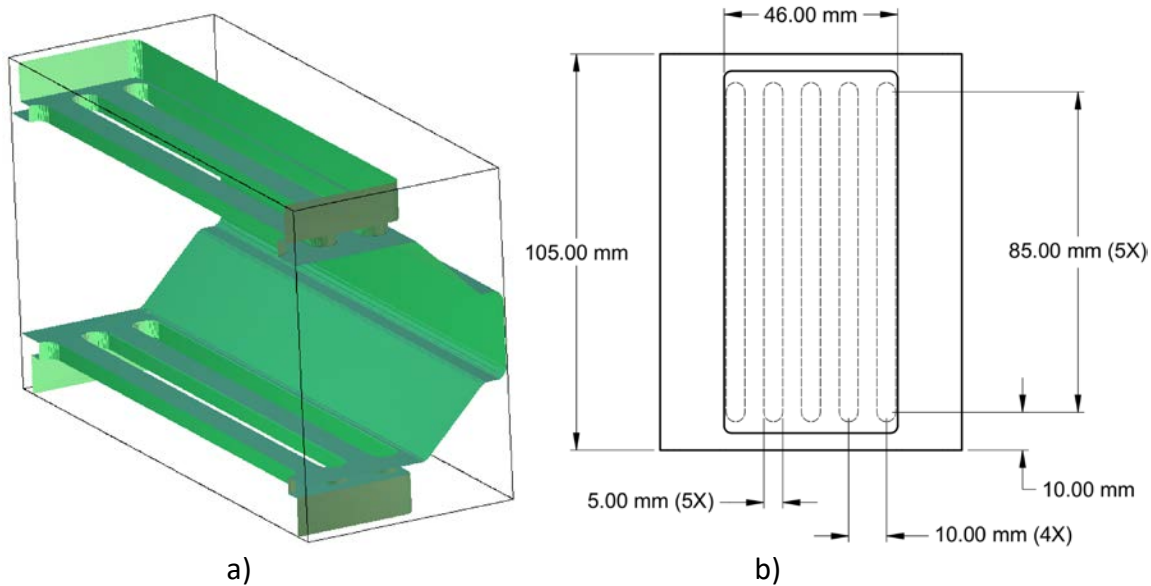


Fig. 3: Standard profile of the electron vacuum chamber with pump slots. a) One-half of the vacuum chamber rendered by the GdfidL code. b) Geometric dimensions of the pump slots.

Figure 4a shows a comparison of the longitudinal wakefield $W_{||}(s)$ for the pump slot arrangement described above (10 slots) vs. the same design with the center slots removed (8 slots). The real part of the longitudinal impedance is presented in Fig. 4b. The low frequency part, up to 8.5GHz , contributes to the heating of the vacuum chamber. The high frequency part is considered for the estimation of the longitudinal microwave instability threshold. Figure 4d shows the loss factor as a function of bunch length. The loss factor for a bunch length $\sigma_s = 12\text{mm}$ is reduced by a factor of 2 for the pump geometry with the center slots.

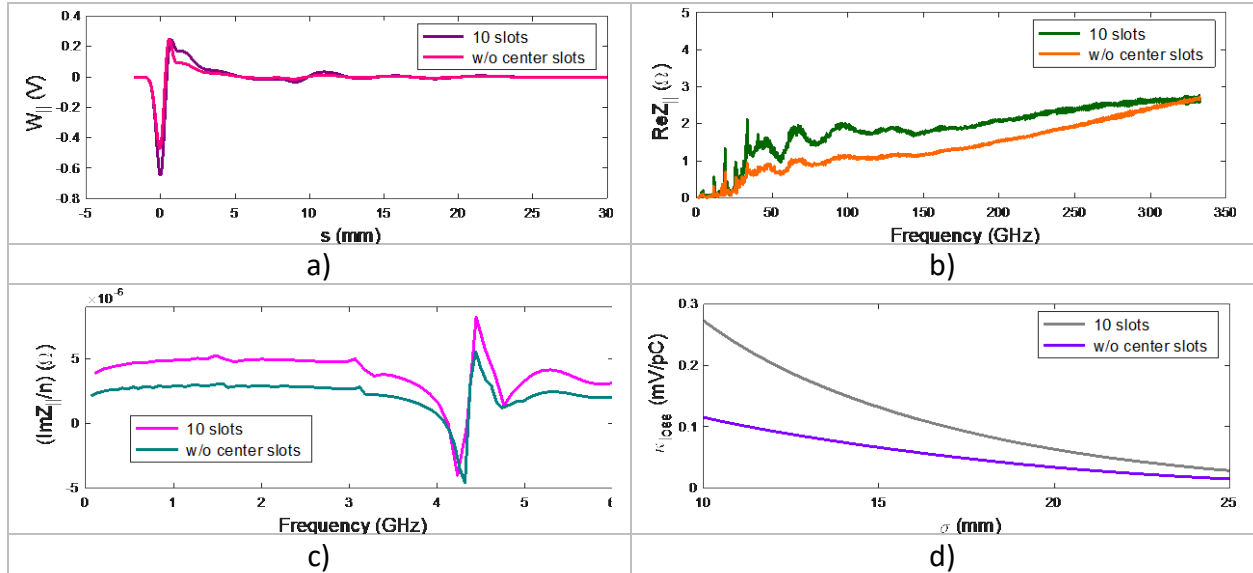


Fig. 4: Pump slots summary results. a) The longitudinal wakepotential simulated for a $\sigma_s = 0.3mm$ bunch length. b) Real part of the longitudinal impedance up to $f = 350GHz$. c) The imaginary part of the longitudinal impedance divided by $n = \omega/\omega_0$, where $\omega_0 = 2\pi \times 78.186kHz$. d) The loss factor as a function of bunch length.

Figure 5 shows a pump slot geometry with double the number of slots but the same longitudinal length. The results for this geometry are summarized in Fig. 6. Since the slot width is still much less than the length of each slot, $w \ll l$, the longitudinal impedance $Z_{||}(\omega)$ at frequencies up to $150GHz$ is twice as large compared to the previous geometry with 8 long slots. The electron beam sees twice as many slots in longitudinal direction which increases $Z_{||}(\omega)$. The loss factor with doubled the number of slots becomes larger for a bunch length $\sigma_s = 12mm$. For $\sigma_s > b$, where $b = 21mm$, $k_{loss}(\sigma_s)$ has the same dependence and the same values (Fig. 6d).

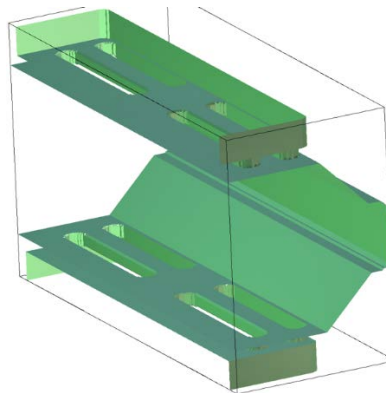


Fig. 5: Standard profile of the electron vacuum chamber with double set of pump slots. One-half of the vacuum chamber rendered by the GdfidL code.

The loss factor with a doubled number of slots becomes larger for a $\sigma_s = 12mm$ bunch length. For $\sigma_s > b$, where $b = 21mm$, $k_{loss}(\sigma_s)$ has the same dependence and the same values (Fig. 6d).

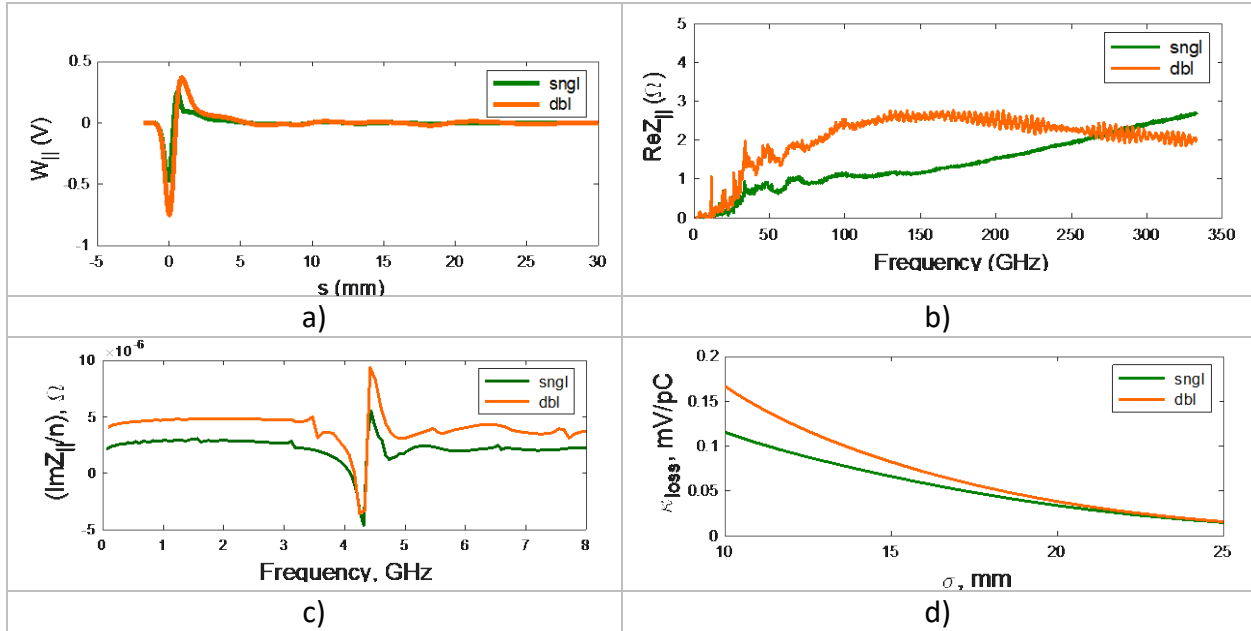


Fig. 6: Pump slots summary results. a) The longitudinal wakepotential simulated for a $\sigma_s = 0.3mm$ bunch length. b) Real part of the longitudinal impedance up to $f = 350GHz$. c) The imaginary part of the longitudinal impedance divided by $n = \omega/\omega_0$, where $\omega_0 = 2\pi \times 78.186kHz$. d) The loss factor as a function of bunch length.

Further improvements can be made by decreasing the width of the slots from 5mm to 3mm. Figure 7 shows two versions of geometry with 3mm slots that were simulated. Figure 7a shows geometry with a total of 12 pump slots. This arrangement provides better conductance to the vacuum pumps. Figure 7b is a rendering of geometry with only 8 pump slots. This arrangement is the same as the previously discussed geometry with 5mm slots except for the change in width. The results are shown in Fig. 8.

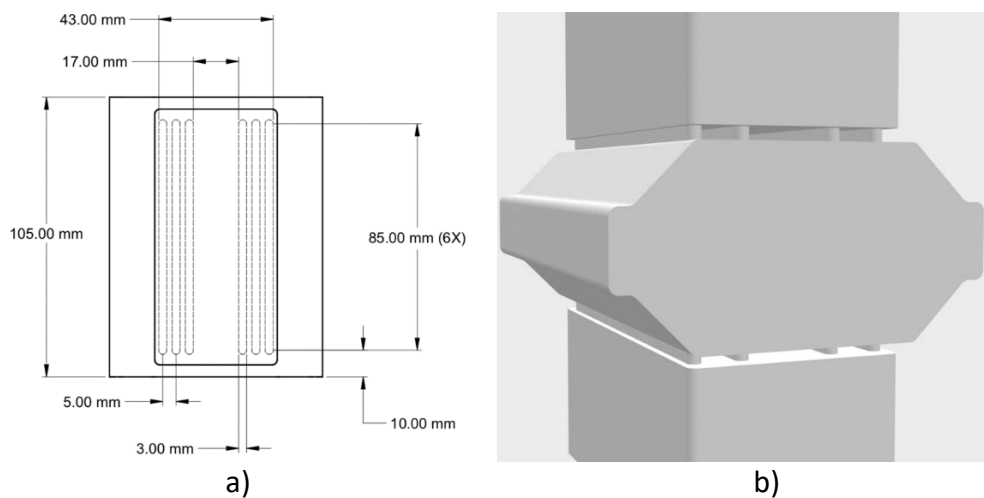


Fig. 7: Standard profile of the EIC vacuum chamber with a) 12 pumping slots and b) 8 pumping slots. The pumping slot width is $w = 3mm$.

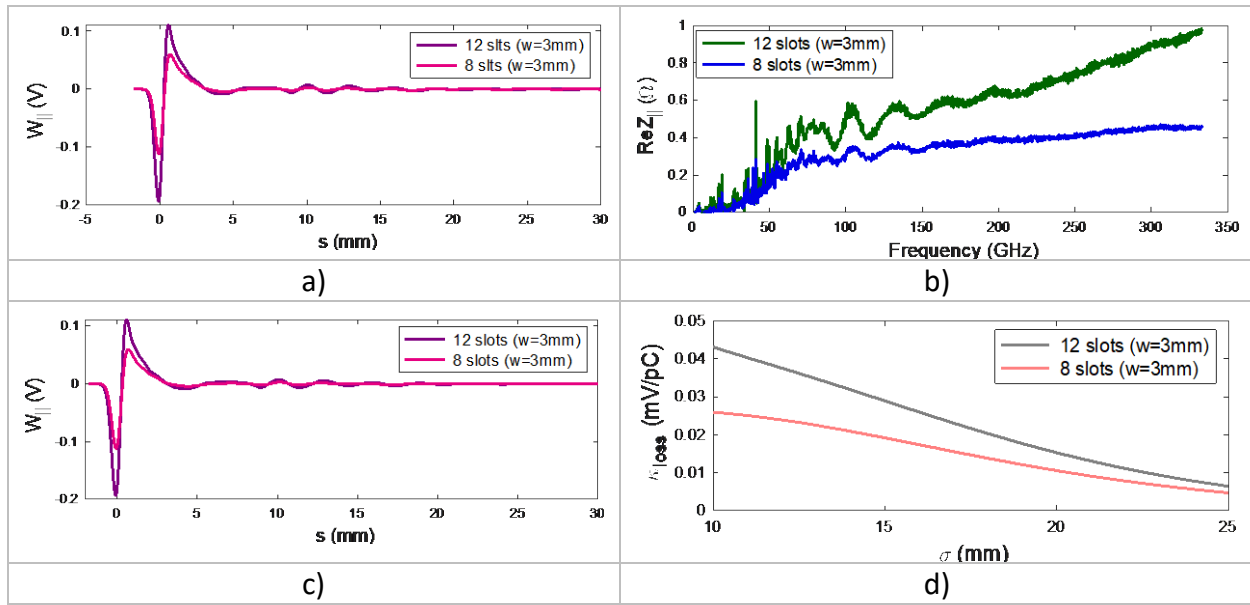


Fig. 8: Pump slots summary results. a) The longitudinal wakepotential simulated for a $\sigma_s = 0.3mm$ bunch length. b) Real part of the longitudinal impedance up to $f = 350GHz$. c) The imaginary part of the longitudinal impedance divided by $n = \omega/\omega_0$, where $\omega_0 = 2\pi \times 78.186kHz$. d) The loss factor as a function of bunch length.

3. IR vacuum chamber

The IR chamber design has been iterated on several times since the eRHIC pCDR. One of the major contributions to the local impedance are discontinuities where the electron and hadron beam pipes merge. The electron pipe geometry needs to be designed so it does not block the propagation of forward moving particles resulting from collisions within a $25mrad$ cone starting from the interaction point. This requirement complicates the transition between the two beam pipes. As a first attempt, the electron beam pipe with a diameter $2d = 62mm$ was grounded to the hadron pipe with a small taper angle. Half of the taper was left open. This arrangement results in a cavity type structure between the area of the electron pipe grounding and the larger hadron beam pipe. The initial taper length was chosen to be 30mm. The results are shown in Figure 10 and labeled ' $L = 30mm$ '.

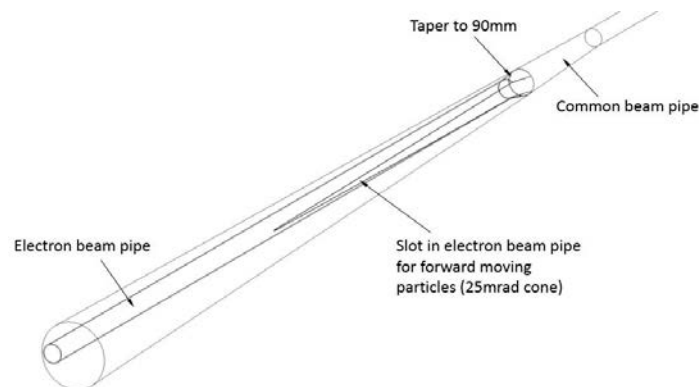


Fig. 9: The EIC IR vacuum chamber design. Version 2

To reduce the cavity effect, the electron beam pipe was extended, and a horizontal slot was added on one side to provide clearance for the particle propagation to the forward detector. The length of the taper was also increased to 90mm. These results are also shown in Figure 10 and are labeled “ $L = 90\text{mm}$ with slot”. Increasing the tapered transition helps to decrease the longitudinal impedance and the loss factor (Fig. 10b and Fig. 10d). The real part of the longitudinal impedance shows existence of the narrow-band impedance at low frequency, generated due to the horizontal slot. The imaginary part of the longitudinal impedance $ImZ_{||}$ divided by $n = \omega/\omega_0$, where $\omega_0 = 2\pi \times 78.186\text{kHz}$, increases slightly. The tapered transition predominantly contributes to the high-frequency impedance. The resonance modes at frequency below 2GHz , have been eliminated by lengthening the tapered transition. However, the horizontal slot contributes to the low-frequency impedance and $(ImZ_{||}/n)_0$ and becomes slightly larger at $f \rightarrow 0$ (Fig. 10c).

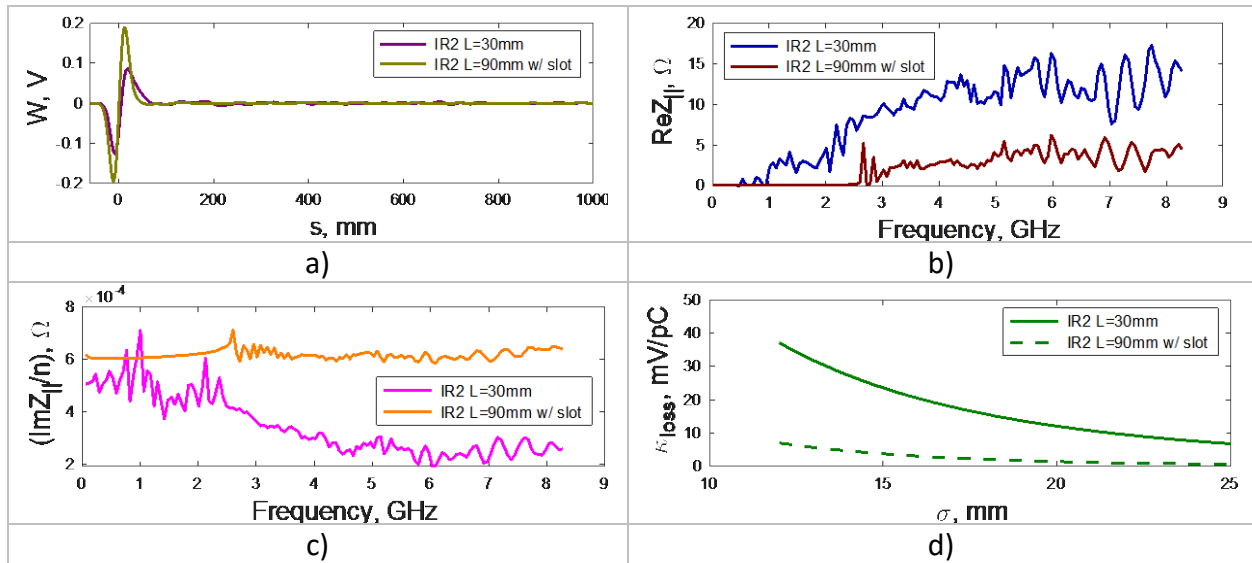


Fig. 10: IR chamber summary results. a) The longitudinal wakepotential simulated for a $\sigma_s = 0.3\text{mm}$ bunch length. b) Real part of the longitudinal impedance up to $f = 350\text{GHz}$. c) The imaginary part of the longitudinal impedance divided by $n = \omega/\omega_0$, where $\omega_0 = 2\pi \times 78.186\text{kHz}$. d) The loss factor as a function of bunch length.

Further refinement to the main detector chamber is shown in Figure 11. The electron beam pipe was extended all the way to the center of the detector chamber. This approach maintains the same diameter all the way to the center of the detector and eliminates the need for a taper. An opening large enough for the forward moving collision particles is added to the side of the electron beam tube. The summarized results are presented in Figure 12. The longitudinal wakefield is shown in Figure 12a and the real part of the longitudinal impedance is presented in Figure 12b. The low-frequency resonance modes around $\sim 3\text{GHz}$ have been eliminated (Fig. 12b) since there is no cavity formed between the 2 beam pipes. The loss factor has also been reduced to $k_{loss} = 2.2\text{mV/pC}$ for a bunch length of $\sigma_s = 12\text{mm}$. The total power loss can be calculated using $P_{loss} = \frac{k_{loss} I_{av}^2 T_0}{M}$. Using the expected average current $I_{av} = 2.48\text{A}$, number of bunches $M = 660$ and the expected revolution period $T_0 = 12.79\mu\text{s}$ the total expected power loss $P_{loss} =$

262 W. This value can be reduced even further by doubling the bunch length. For a bunch length $\sigma_s = 24mm$, the power loss factor drops by almost a factor of 10 to $k_{loss} = 0.2mV/pC$ resulting in a total power loss $P_{loss} = 30W$.

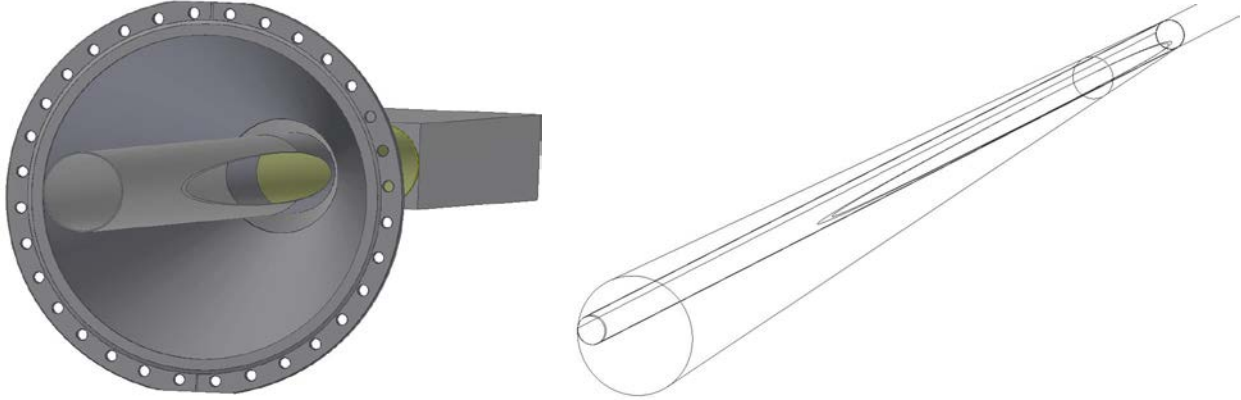


Fig. 11: The EIC IR vacuum chamber design. Version 3.

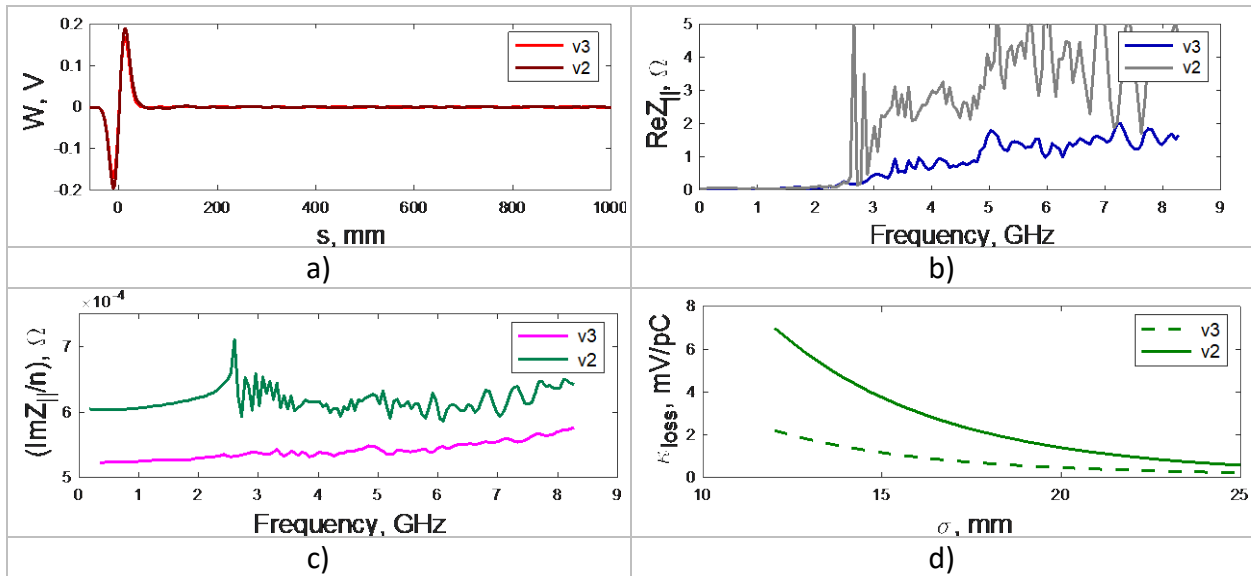


Fig. 12: Summary results for IR chamber v3. a) The longitudinal wakepotential simulated for a $\sigma_s = 0.3mm$ bunch length. b) Real part of the longitudinal impedance up to $f = 350GHz$. c) The imaginary part of the longitudinal impedance divided by $n = \omega/\omega_0$, where $\omega_0 = 2\pi \times 78.186kHz$. d) The loss factor as a function of bunch length.

4. Transition from the octagonal dipole chamber to the circular straight section chamber

To minimize contribution to the total impedance of the ring, a tapered transition (Fig. 13) is applied from the octagonal shape of the arc vacuum chamber (half-aperture $h = 20mm$) to the circular profile of the straight section vacuum chamber (radius $b = 31mm$). The summary results for the tapered transition with length $L = 180mm$ are presented in Fig. 14.

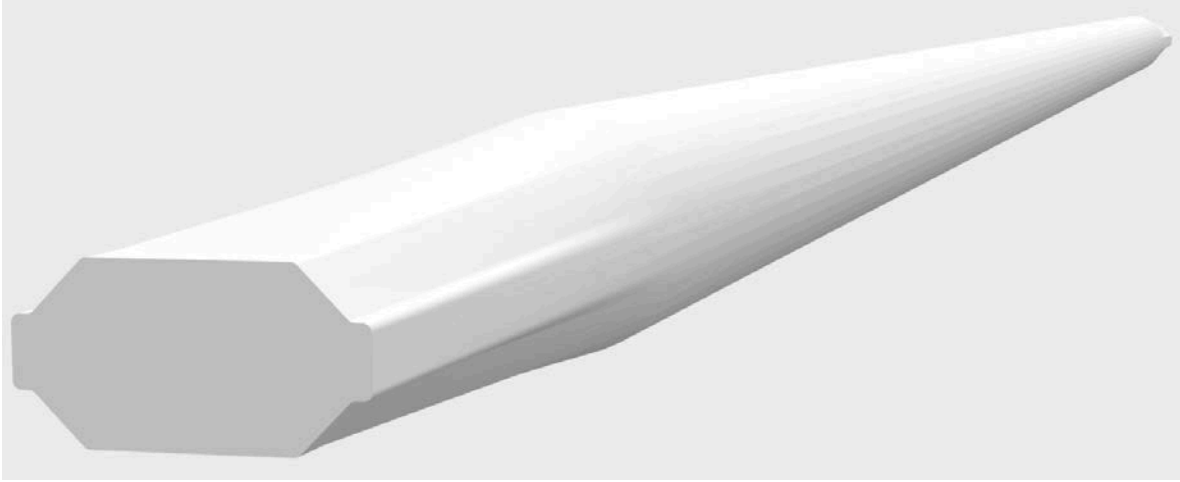


Fig. 13: Tapered transition of the vacuum chamber from the octagonal to the circular shape.

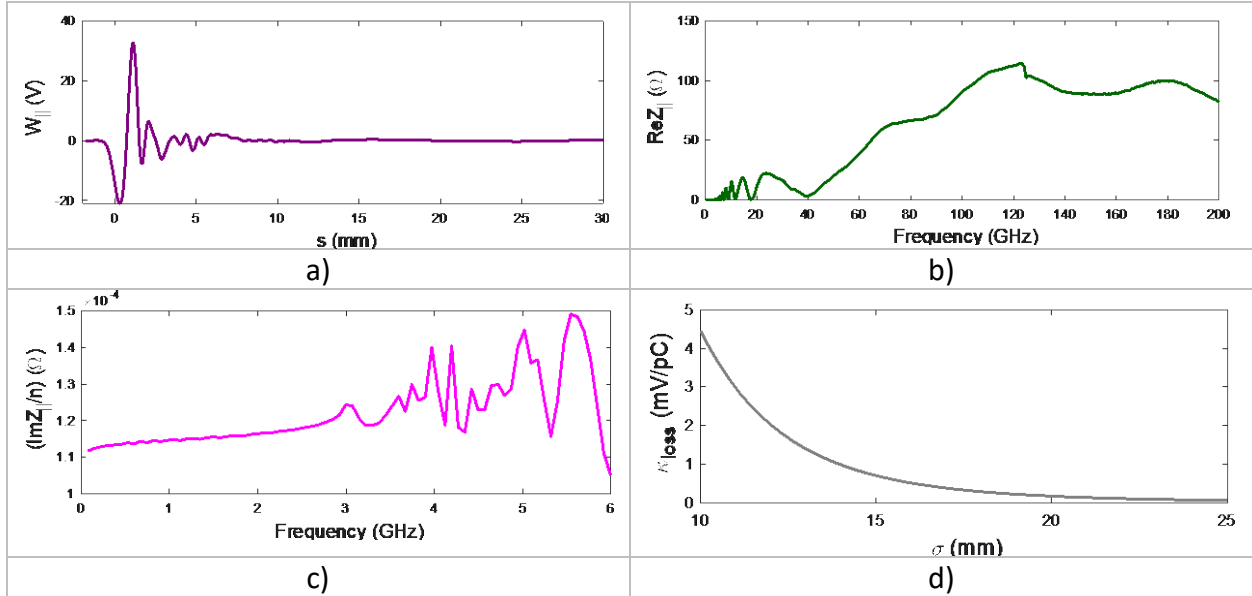


Fig. 14: Tapered transition from the arc vacuum chamber to the straight section vacuum chamber. a) The longitudinal wakepotential simulated for a $\sigma_s = 0.3mm$ bunch length. b) Real part of the longitudinal impedance up to $f = 350GHz$. c) The imaginary part of the longitudinal impedance divided by $n = \omega/\omega_0$, where $\omega_0 = 2\pi \times 78.186kHz$. d) The loss factor as a function of bunch length.

Due to changes in the vertical and the horizontal dimensions, the considered model can be presented as a cavity type structure, where the first resonance mode is defined by the largest radius in the structure. The cutoff frequency for the E_{01} -mode, like in a circular waveguide, for $b = 31mm$ is $f_{c,E01} = 3.7GHz$ (Eq.(1)). Based on the straight section length, we can identify the frequencies of E_{01p} -mode (like in a cavity structure), where p is the number of field variations in z-direction. The loss factor k_{loss} for a $\sigma_s = 12mm$ is $k_{loss} = 2mV/pC$ (Fig. 14d). The power loss

is $P_{loss} = 238W$. This power loss can be eliminated if the same vacuum chamber cross section can be used in both the arcs and the straight sections.

5. Concluding remarks

In this Technote we discuss the profile of the vacuum chamber for the future EIC project. Since the average current is designed to be $I_{av} = 2.4A$, the vacuum chambers need to be designed with less discontinuities as possible to avoid any localized heating's issues. One of the main key components is the IR chamber. To avoid generation of the trapped modes inside the IR chamber, the diameter of the attached beam pipes should be increased and be bigger than the diameter of the central part. In this case the different modes can propagate outside of the central part of the IR chamber. The diameter of the outgoing pipes should match the profile of the standard vacuum chamber, otherwise some reflected modes will be generated, and those modes will be contributing to the localized heating of the IR chamber. The Higher Harmonic Cavity installation will be strongly beneficial for the bunch lengthening, since it will be useful in raising the longitudinal microwave instability threshold and reducing the heat load due to the image current.

Contribution of the considered vacuum components to the total longitudinal impedance of the ring is summarized in Table 1.

Table 1: Summary of longitudinal impedance contributions

Element	Number	$\Sigma(ImZ_{ }/n)_0,$ $m\Omega$
Pump slots (8 slots, w=3mm)	500	0.3
Tapered transition (DM to SS)	8	0.9
IR chamber (IR chm)	1	0.5
Total:		1.7

We will be using the impedance model, with more components added, to describe various collective effects in EIC in near future.

REFERENCES

[1] W. Bruns, <http://www.gdfidl.de>